Cell Reports
Physical Science

CellPress
OPEN ACCESS

Article

Efficient generation of emissive many-body correlations in copper-doped colloidal quantum wells

Junhong Yu,[1,10] Manoj Sharma,[1,7,10] Mingjie Li,[2,8,10] Baiquan Liu,[3,*]
Pedro Ludwig Hernández-Martínez,[1,4] Savas Delikanli,[1,4] Ashma Sharma,[1] Yemliha Altintas,[4,9]
Chathuranga Hettiarachchi,[5] Tze Chien Sum,[2] Hilmi Volkan Demir,[1,2,4,*] and Cuong Dang[1,5,6,11,*]

SUMMARY

Colloidal quantum wells (CQWs) provide an appealing platform to achieve emissive many-body correlations for novel optoelectronic devices, given that they act as hosts for strong carrier Coulomb interactions and present suppressed Auger recombination. However, the demonstrated high-order excitonic emission in CQWs requires ultrafast pumping with high excitation levels and can only be spectrally resolved at the single-particle level under cryogenic conditions. Here, through systematic investigation using static power-dependent emission spectroscopy and transient carrier dynamics, we show that Cu-doped CdSe CQWs exhibit continuous-wave-pumped high-order excitonic emission at room temperature with a large binding energy of ~64 meV. We attribute this unique behavior to dopant excitons in which the ultralong lifetime and the highly localized wavefunction facilitate the formation of many-body correlations. The spectrally resolved high-order excitonic emission generated at power levels compatible with solar irradiation and electrical injection might pave the way for novel solution-processed solid-state devices.

INTRODUCTION

Many-body correlations studies (or the higher-order correlated excitonic state) comprise a fascinating topic that has attracted decades of experimental and theoretical investigations due to its high technical relevance to optoelectronic and quantum information applications.[1,2] For instance, biexcitons (excitonic molecules) are beneficial for both optical gain performance (i.e., biexcitons provide a four-energy-level scheme to achieve low-threshold lasing)[3] and entangled photon pair generation (i.e., the cascade emission of a biexciton automatically generates a polarization-entangled photon pair)[4,5]; While the spin of the extra charge in a trion (the charged exciton) can essentially be utilized as a natural two-level quantum system for the novel design of quantum information devices (including quantum repeaters, quantum switches, and quantum memories).[6–8] Colloidal quantum wells (CQWs) have attracted tremendous interest in this regard thanks to their strong exciton center-of-mass localization,[9,10] giant exciton oscillator strength,[11–13] and reduced dielectric screening.[14–16] These advantages lead to ultra-stable excitonic complexes, providing a promising platform for the investigation of many-body correlations. Although substantial efforts (e.g., engineering the wavefunction, confinement potential, or material compositions)[3,6,17–21] have been made to harvest the trion/biexciton emission for potential applications, all reported demonstrations still require high excitation levels with an ultrashort pulsed laser; and, most annoyingly,

[1]LUMINOUS! Centre of Excellence for Semiconductor Lighting and Displays, School of Electrical and Electronic Engineering, Nanyang Technological University, 50 Nanyang Avenue, Singapore 639798, Singapore

[2]School of Physical and Mathematical Sciences, Nanyang Technological University, Singapore 639798, Singapore

[3]School of Electronics and Information Technology, Sun Yat-sen University, Guangzhou 510275, China

[4]Department of Electrical and Electronics Engineering and Department of Physics, UNAM-Institute of Materials Science and Nanotechnology, Bilkent University, Bilkent, Ankara 06800, Turkey

[5]Centre for OptoElectronics and Biophotonics, School of Electrical and Electronic Engineering & The Photonics Institute, Nanyang Technological University, 50 Nanyang Avenue, Singapore 639798, Singapore

[6]CINTRA UMI CNRS/NTU/THALES 3288, Research Techno Plaza, 50 Nanyang Drive, Border X Block, Level 6, Singapore 637553, Singapore

[7]ARC Centre of Excellence in Exciton Science, Department of Materials Science and Engineering, Monash University, Clayton Campus, Melbourne, VIC 3800, Australia

[8]Department of Applied Physics, The Hong Kong Polytechnic University, Hung Hom, Kowloon, Hong Kong, China

[9]Department of Material Science and Nanotechnology Engineering, Abdullah Gul University, Kayseri 38080, Turkey

[10]These authors contributed equally

[11]Lead contact

*Correspondence:
liubq33@mail.sysu.edu.cn (B.L.),
volkan@stanfordalumni.org (H.V.D.),
hcdang@ntu.edu.sg (C.D.)

https://doi.org/10.1016/j.xcrp.2022.101049

the many-body correlated emission band is largely overlapped with the exciton emission profile, which only allows for spectrally resolved emission at the single-particle level under cryogenic conditions.[3,6,19,20]

In this work, we propose that "dopant excitons" in Cu-doped CdSe CQWs have great potential to resolve the above-mentioned challenges. The long-lived trapped excitons permit several orders of magnitude enhancement in their density compared with short-lived band-edge excitons under the same continuous-wave (CW) excitation,[22,23] rendering the many-body correlations much more efficiently to form. Meanwhile, trapped excitons have highly localized wavefunctions with well-defined energy levels pinned at the Cu^{+}/Cu^{2+} redox potential.[24] The interaction strength (or the binding energy) is greatly enhanced when trapped excitons are correlated with band-edge carriers/excitons,[25] possibly resulting in the spectrally resolvable emission lines at room temperature. To verify this conjecture, we have investigated both the static emission properties and the transient carrier dynamics of Cu-doped CdSe CQWs. CW-pumped and well-resolved many-body correlations at room temperature have been unambiguously identified by two following fingerprint-like features. Static results reveal that a new emission line appears under CW excitation above ~10 W/cm^2 with a giant binding energy of ~64 meV and the intensity quadratically scaling with the pump intensity. Transient measurements confirm that the newly excited species exhibit delayed and accelerated recombination dynamics compared with the band-edge excitons, which radiatively recombine via stimulated emission (SE). Our works now push the realization conditions for emissive many-body correlations to very practical levels suitable for solar irradiation or direct electrical injection.

RESULTS AND DISCUSSION

Cu-doped colloidal CdSe quantum wells

The 4.5 monolayers (4.5 ML, 5 Cd, and 4 Se layers) Cu-doped CdSe CQWs studied here are prepared according to the existing recipe[26–29] with optimized procedures to achieve highly efficient and reproducible synthesis (details of the modified recipe are described in Note S1). The average number of copper dopants per CQW, $<N_{Cu}>$, is determined by inductively coupled plasma mass spectrometry (ICP-MS, see details in experimental procedures).[27] For the following experiments, CQWs with $<N_{Cu}>$ = ~40 Cu (i.e., corresponding to 0.23% Cu atomic percentage) and a quantum yield of ~60% are investigated. Figure 1A shows the transmission electron microscopy (TEM) image of the Cu-doped CQWs, which have an approximately rectangular shape with uniform size distribution. Typical static absorption and photoluminescence (PL) spectra of Cu-doped CQWs under UV illumination are shown in Figure 1B. The absorption spectrum (the blue curve) of Cu-doped CQWs remains nearly unchanged compared with undoped CdSe CQWs[3,16]: two apparent excitonic features associated with electron to heavy-hole (~512 nm) and electron to light-hole (~480 nm) transitions are observed. While the PL spectrum (the black curve) of Cu-doped CQWs is composed of band-edge emission (BE) (shaded in green) and Cu-related emission (CE) (shaded in red). BE is centered at ~514 nm with a full-width at half-maximum (FWHM) of ~40 meV, which is not affected by copper dopants (i.e., similar to undoped CQWs), while CE peaks at ~700 nm with a very large FWHM of ~350 meV. It is well-known that the broad emission linewidth arises from a wide distribution of the copper energy levels and strong electron-phonon coupling rather than size/doping inhomogeneity within an ensemble of Cu-doped CdSe CQWs, as detailed previously.[30–34]

The emission mechanism of Cu-doped CQWs is illustrated in Figure 1C. After excitation, copper dopants irreversibly localize the photo-generated holes in the valance

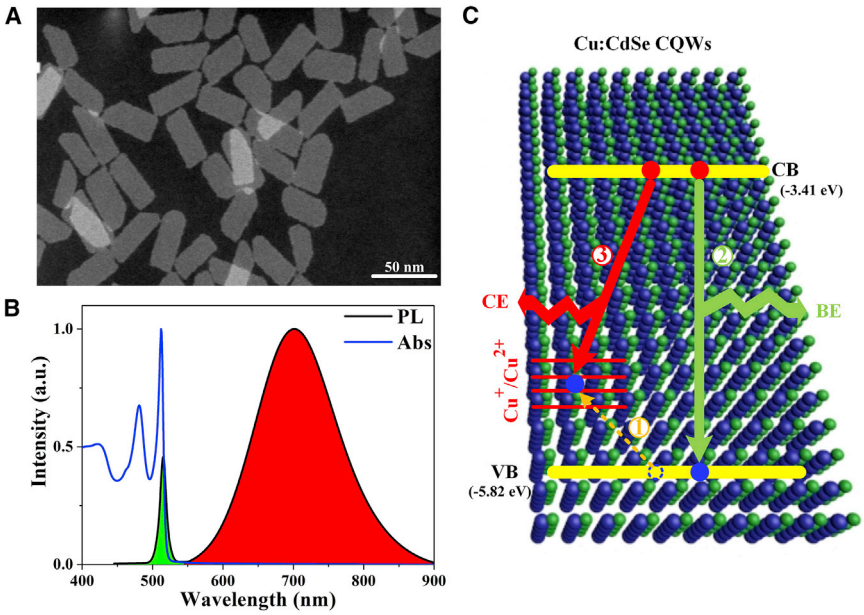

Figure 1. Cu-doped CdSe colloidal quantum wells

(A) Transmission electron microscopy image of Cu-doped CdSe colloidal quantum wells (CQWs).

(B) Absorption and PL spectrum of Cu-doped CQWs in hexane under xenon lamp illumination; the green-colored region indicates the band-edge emission (BE) and the red-colored region indicates the copper-related emission (CE).

(C) Schematic of carrier dynamics in the Cu-doped CQWs with photoexcitation. After capturing a valance band hole (process 1), Cu^{+} is changed to Cu^{2+}, activating the CE through recombining with a CB electron (process 3).

band of the CdSe CQW host (Cu^{+} is promoted to Cu^{2+}), while the electrons mostly reside at the conduction band (CB) edge.[29,35] Thereafter, dopant excitons (formed between the captured hole in copper sites and the electron resident at the CB edge) recombine radiatively, resulting in the CE band.[24,28] Being aware of the attractive features carried by dopant excitons as described below, we realize that Cu-doped CdSe CQWs could be an ideal system to demonstrate the emissive many-body correlations: (1) due to the reduced electron-hole wavefunction overlap,[24,27,30] dopant excitons exhibit a lifetime (~450 ns, see Figure S1) that is several orders of magnitude longer than the band-edge exciton (~290 ps, see Figure S2); therefore, the steady-state density of trapped excitons can be much higher than that of band-edge excitons for CW excitation based on the steady-state kinetic equation $N = P \times \tau$ (where N is the exciton density, P is the exciton generation factor, and τ is the recombination lifetime)[5,22]; (2) dopant excitons have localized wave functions with energy levels roughly pinned at the Cu^{+}/Cu^{2+} redox potential.[24,35] This strong spatial confinement greatly enhances the Coulomb correlation effect when CB electrons or band-edge excitons diffusively approach dopant excitons, resulting in a high formation rate and large binding energy.[s]

Static evidence of emissive many-body correlations

We have investigated the PL of Cu-doped CQWs under CW excitation with different intensities at room temperature (see Figures 2A and 2B). With low excitation intensity (<6 W/cm^2, the bottom spectrum in Figure 2B), the BE shows a single symmetric peak at ~514 nm, which is the typical single exciton emission observed in 4 ML CdSe CQWs. With gradually increased excitation intensity, a new emission feature appears at the low energy side (peaking at ~528 nm) and the intensity of this new

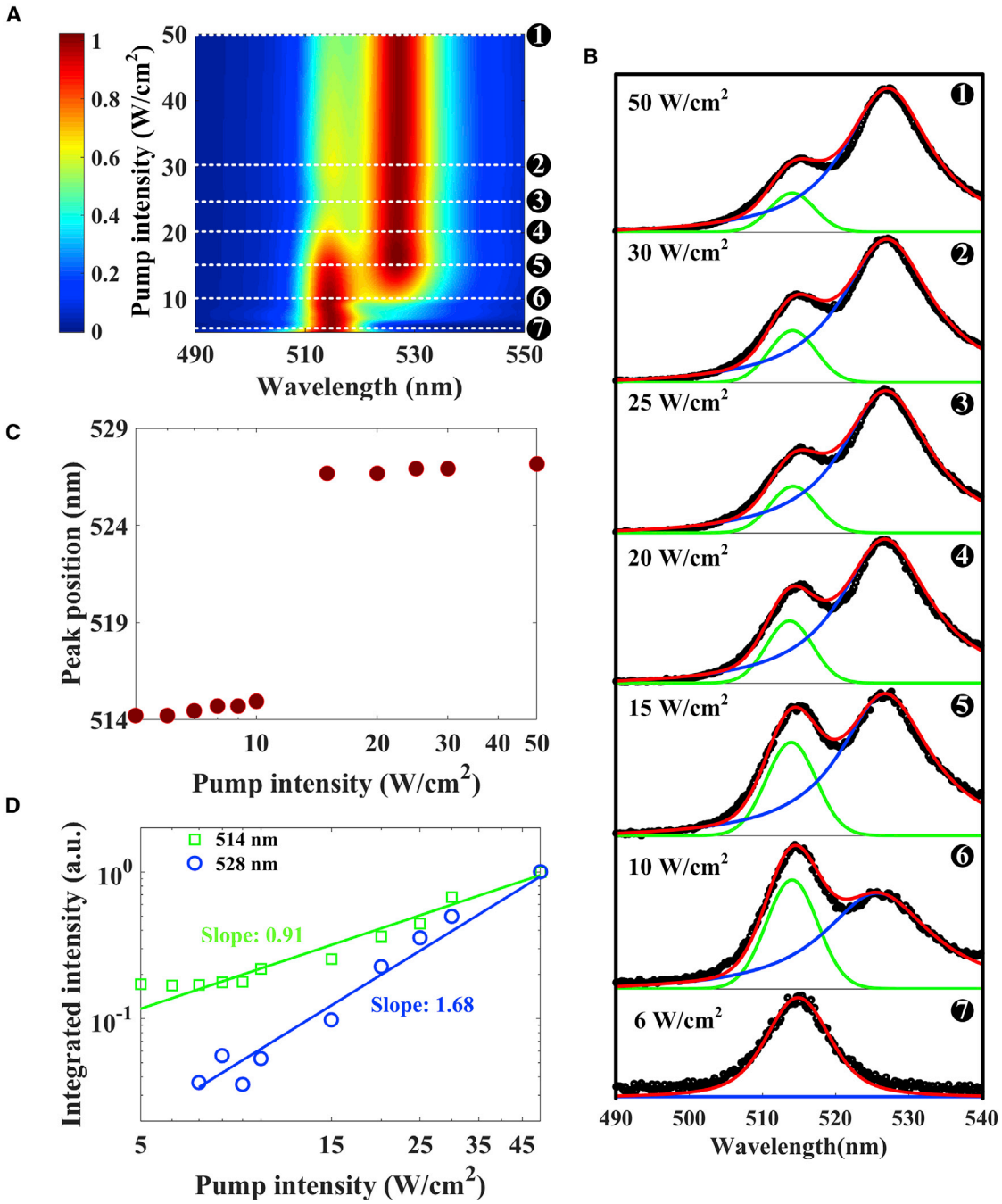

Figure 2. PL spectra of Cu-doped CQWs at room temperature with varied CW excitation intensities

(A) Normalized BE map of Cu-doped CdSe CQWs under different excitation intensities. The white dashed lines indicate different excitation intensities, and the ordered numbers correspond to the BE spectra in (B).

(B) BE spectra recorded for different excitation intensities. Black dots: experimental data; green line: the fitting of exciton emission; blue line: the fitting of biexciton emission; red line: the overall fitting.

(C) The wavelength of the maximum BE intensity as a function of the excitation intensity. Beyond ~10 W/cm^2, the emission intensity peaked at ~528 nm, which exceeds that of the exciton emission, which peaked at ~514 nm.

(D) The logarithmic plot of integrated intensities for the emission band peaked at 514 nm (green squares) and 528 nm (blue circles) as a function of the excitation intensities. The green and blue solid lines are the power-law fittings. Please note that the integrated intensities for each emission band are normalized.

feature grows much faster than that of exciton emission at 514 nm (see Video S1). Beyond the excitation intensity of ~10 W/cm^2, the new feature emerges as the strongest emission channel (see Figure 2C, the maximum intensity of BE shifts from 514 to 528 nm with higher excitation intensity). As for the origin of this emerged emission band in Cu-doped CQWs, we can easily exclude the possibility of inhomogeneous doping or aggregation (i.e., stacking) in the solid-state film. First, enormous works on doped CQWs have demonstrated that transition metal ions (e.g., Cu^+, Mn^{2+}, Ag^+, Hg^{2+}) induced by a chemical doping process are located uniformly inside each host CQW by substitution host cations.[30–35] Our previous works have conducted energy-dispersive X-ray spectroscopy mapping, which clearly shows the homogeneous doping of Cu atoms within the core CQWs.[27,29] Second, the stacking of CQWs will result in a significant quenching of the BE emission due to the exciton hopping (i.e., the homo-nonresonant energy transfer among the stacking) boosted the hole-trapping process[18,28,36] and the observation of similar emission behavior in solutions has further ruled out the role of energy transfer in long-range stacked CQWs (see Figure S3). Most importantly, the threshold behavior and a faster-increasing rate strongly suggest that the emerged emission feature is generated from the radiative recombination of newly excited species distinct from excitons.

Since the intensity scaling is often used as a unique criterion to identify many-body correlations,[5,22,37] we have fitted BE with two separately symmetric profiles using the Voigt function[3,38] to spectrally separate the 514 and 528 nm emission features (as shown in Figure 2B). The fitting profiles are in good agreement with the experimental spectra at various excitation intensities. Figure 2D presents the excitation intensity dependence of these two features, which can be described adequately by the power-law equation[5,37]: $I_{emission} \propto I_{excitation}^{k}$. The exciton emission at 514 nm exhibits a slightly sublinear fluence dependence (k = 0.91), due to the hole capturing process from host CQWs to Cu^+ sites.[28,30] In contrast, the integrated intensity of the emerged low-energy emission displays a super-linear growth with the excitation intensity (k = 1.68). Compared with the emission of the exciton species at ~514 nm, which increases nearly linearly with laser intensity, the quadratic intensity dependence (1.68/0.91 = 1.85) strongly suggests that the emission peak at ~528 nm is arising from a second-order excitonic state.[5,22,37] For the nature of this high-order excitonic state, we can safely rule out the possibilities of biexcitons being composed of two dopant excitons due to the negative binding energy requirement[22,23] and trions/biexcitons being composed of pure band-edge carriers due to the ultralow steady-state density at 10 W/cm^2 (a kinetic model is presented in Note S2 to describe the biexciton and trion formation processes). It is worth mentioning that, at this stage, we cannot pinpoint whether the second-order excitonic emission is originating from a dopant trion (i.e., the Coulomb bounding between a dopant exciton and an electron in the CB of the CdSe host) or a dopant biexciton (i.e., the Coulomb bounding between a dopant exciton and a band-edge exciton) because the formation of both requires the excitation of two components, each exhibiting a concentration growing linearly with the excitation intensity. Nonetheless, we posit that time-correlated single-photon counting[39] or circular emission polarization in magnetic field[19] could help to reveal the constituent of the observed many-body correlations in Cu-doped CQWs, which is beyond the scope of this work. It is worth mentioning that we have also checked the thermal stability of observed many-body correlations in Cu-doped CdSe CQWs at the excitation intensity of 10 W/cm^2 and temperature-dependent emission spectra further verify the extracted binding energy (see details in Figure S4).

Meanwhile, we should emphasize that this observation constitutes the first demonstration of CW-pumped emissive many-body correlations in the colloidal nanocrystal

family. It also shows the possibility of distinguishably harvesting emitted photons from the high-order excitonic state in colloidal semiconductors with the status of solid-state films at ambient conditions. Specifically, the excitation intensity of ~10 W/cm^2 is at least three orders of magnitude lower than the value in typical colloidal nanocrystals employing pulsed laser excitation.[3,6] Such an ultralow excitation intensity can be directly compared with the electron density injection in state-of-the-art DC-driven, electroluminescent colloidal nanocrystal-based light-emitting diodes (10 W/cm^2 correspond to an electrical DC density of approximately 5 A/cm^2 and the injected current density is already up to 18 A/cm^2 in Klimov's works[40]) and matches the power density of concentrated solar irradiance (the intensity of a focused sunlight spot can be easily above 50 W/cm^2).[41] In parallel, the extracted binding energy with a value of ~64 meV (see the binding energy calculation in experimental procedures) is 2-fold of that observed in undoped CdSe CQWs (see PL spectra of undoped CdSe CQWs in Figure S5).[3,6,19,20] It is also higher than that of inorganic colloidal perovskites[4] and comparable with the values measured in monolayer transition metal dichalcogenides,[5,22,42] which further renders the potential of Cu-doped CQWs for practical device applications.

Dynamic evidence of emissive many-body correlations

To further validate the emissive many-body correlations, we have investigated the carrier dynamics in Cu-doped CQWs. First, we conduct time-resolved emission measurements with varying excitation fluences (see experimental details in experimental procedures). As shown in the bottom panel of Figure 3A, a narrow PL spectrum is observed with a low excitation fluence (0.4 μJ/cm^2), and the emission peak (the hottest spot in the 2D contour map) is located at ~514 nm. However, at a higher fluence (40 μJ/cm^2, see the top panel of Figure 3A), the emission spectrum becomes much broader and the peak shifts to the wavelength at ~528 nm, consistent with the observation in CW excited steady-state emission spectra. Following the white and red dashed lines in Figure 3A, we compare the emission decay trace at wavelengths of 514 and 528 nm. With low fluences in which the biexciton emission is absent (see Figure 3B), the dynamics at 514 and 528 nm are almost identical (single-decay process with a similar lifetime of ~234 ± 14 and ~245 ± 36 ps for 514 and 528 nm, respectively). In contrast, with a higher fluence of 40 μJ/cm^2 (see Figure 3C), the emission channel located at 528 nm displays a faster recombination rate with a lifetime of 127 ± 16 ps, while the lifetime of the emission channel located at 514 nm is still 203 ± 18 ps. Besides the accelerated recombination dynamics, we have also noticed that, at 40 μJ/cm^2, the onset of the emission line peaked at 528 nm and is slightly delayed compared with the excitonic emission at 514 nm, which again suggests that the new emission band is originating from high-order excitonic states (e.g., the delayed emission onset from biexcitons or trions is usually observed in bulk or high-quality quantum wells, where many-body correlations are formed by combining multiple carriers).[3,43,44]

It is widely established that high-order excitonic states (e.g., trions or biexctions) can generate SE signals in the pump-probe experiment due to fulfilment of the population inversion condition.[45–47] Therefore, another dynamic evidence to support the assignment of high-order excitonic states is the observation of optical gain at high excitation fluence in transient-absorption measurements (see experimental procedures for details). In Figure 4, we focus on the change in absorbance ΔA at a wavelength range near 528 nm with a excitation fluence of 40 μJ/cm^2 (a colored map across the full wavelength range, which also shows the heavy and light exciton bleaching, is provided in Figure S6). As expected, we observe a weak absorption bleach due to the $ML_{CB}CT$ process (the sub-band gap copper-to-CB charge transfer

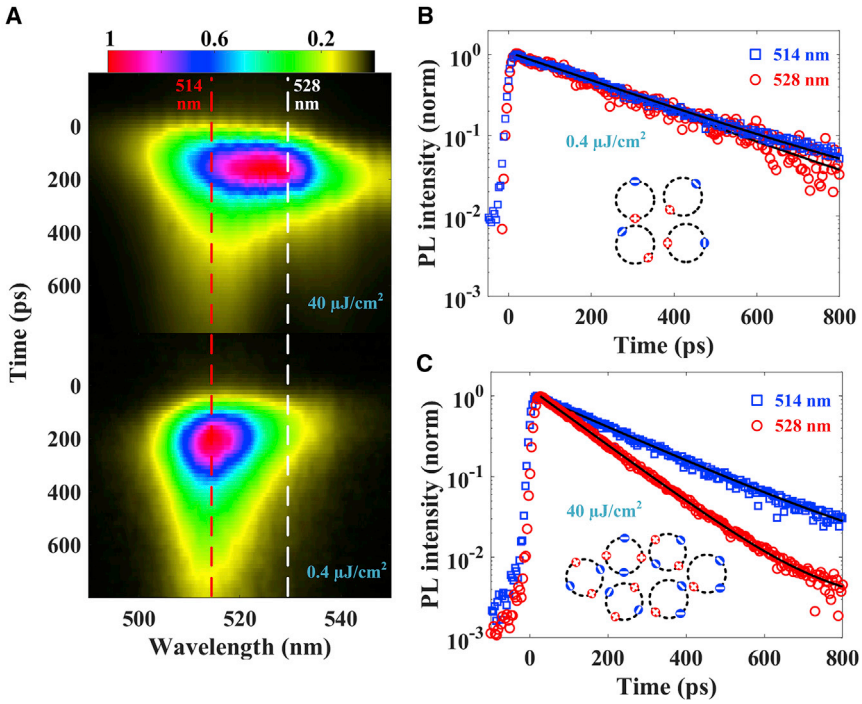

Figure 3. Time-resolved emission spectrum of Cu-doped CQWs

(A) Streak camera images of Cu-doped CdSe CQWs under excitation of 100 fs pulsed laser. Top panel: at high excitation fluence (40 μJ/cm^2) in which high-order excitonic emission is observed. Bottom panel: at low excitation fluence (0.4 μJ/cm^2) in which only BE is observed. The red dashed line is located at 514 nm and the white dashed line is located at 528 nm.

(B) Decay traces probed at 514 and 528 nm and corresponding fitting curves when the excitation fluence is 0.4 μJ/cm^2. 514 nm (measurement, blue squares; fitting, black solid line), 528 nm (measurement, red circles; fitting, black solid line).

(C) Decay traces probed at 514 and 528 nm and corresponding fitting curves when the excitation fluence is 40 μJ/cm^2; the same color and shape coding for data as in (B).

process and details of this transition can be found in the works of Gamelin and co-workers[30,35]) in the ΔA spectra of Cu-doped CQWs, which covers the whole spectrum beyond the red side of the positive photo-induced absorption (PIA) band (see the top panel of Figures 4A and 4B). This weak absorption bleach exhibits nearly invariant dynamics within the measured time window (>3 ns), which is consistent with the slow recombination rate between CB electrons and copper-trapped holes (lifetime: ~450 ns; see Figure S1). Notably, after several picoseconds delay, we unambiguously observe the appearance of a strong negative signal (the saturated red region in the top panel of Figure 4A) peaked at ~528 nm below the PIA band. Please note that this negative band at 528 nm cannot be observed in undoped CdSe CQWs at the same excitation level (see the comparison between Cu-doped and doped samples in Figure S6). We here assign the emerged negative signal around 528 nm to an SE process related to more than one exciton in a CQW because of the following reasons: (1) the strong negative signal neither corresponds to any resonant transition features in the host CQWs nor the $ML_{CB}CT$ process; (2) the strong negative signal shows a delayed formation and only appears after several picoseconds (see Figure 4B) with respect to the excitonic and the $ML_{CB}CT$ bleaching band; (3) the negative signal can only be observed with high pump fluence (see the ΔA in Cu-doped CdSe CQWs with different pump fluences in Figure S7), and the energy location exactly matches our biexciton emission spectra. Please note

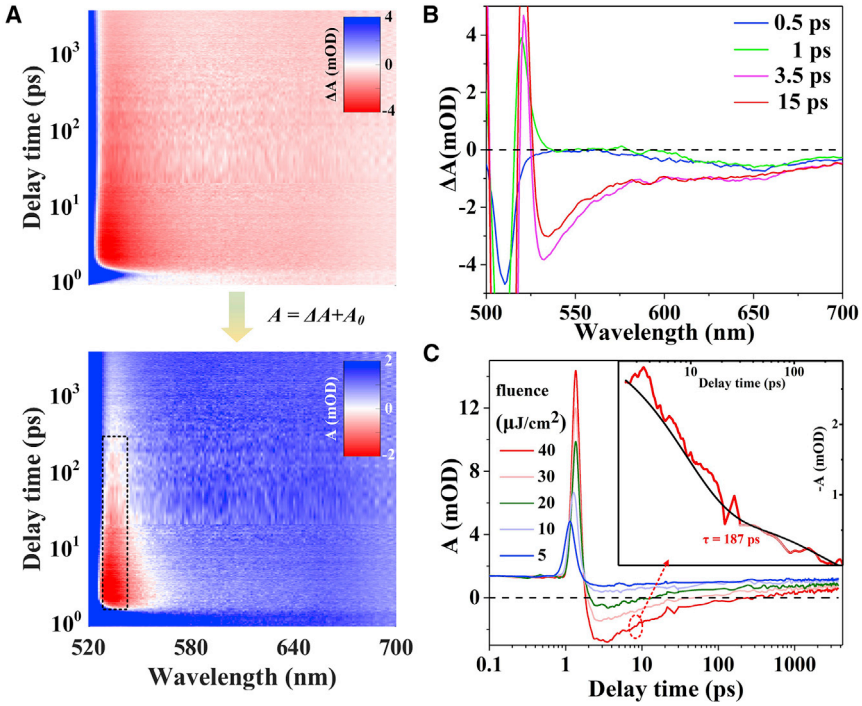

Figure 4. Transient absorption spectra of Cu-doped CdSe CQWs; excitation laser: 100 fs at 400 nm

(A) Top panel: 2D transient absorption change (ΔA) images of Cu-doped CdSe CQWs. The measurement is obtained at a fluence of 40 μJ/cm^2. Bottom panel: 2D transient absorption (A) images of Cu-doped CdSe CQWs at a fluence of 40 μJ/cm^2. The red color-coded region indicates the stimulated emission ($A < 0$) around 528 nm.

(B) ΔA spectra as a function of the wavelength at different delay times with a fluence of 40 μJ/cm^2. The negative band around 528 nm exhibits a delayed formation.

(C) Time-resolved A spectra (probed at 528 nm) with different fluences. At a fluence of 40 μJ/cm^2, the gain can last over a period of >200 ps. The inset shows the dynamics of $-A$ at a fluence of 40 μJ/cm^2, which yields a lifetime of 187 ± 5 ps.

that the reason for optical gain detected in pump-probe experiments from the solution of Cu-doped CQWs is that photons produced by SE are identical (phase, energy, and momentum) to the probe photons, different from those produced by spontaneous emission.[45]

The optical gain from high-order excitonic states is further verified by the absolute absorbance $A(\lambda,t) = \Delta A(\lambda,t)+A_0(\lambda)$, where $A_0(\lambda)$ is the linear absorption with the same measurement condition.[46] The bottom panel of Figure 4A presents the color map of absolute absorbance at a pump fluence of 40 μJ/cm^2, which codes the positive absorbance with blue color and gain ($A<0$) with red color. The optical gain region agrees very well with the biexciton emission resolved in previous parts (dashed black rectangle) and can last more than 100 ps. The dynamics of SE under different pump fluences probed at the wavelength of 528 nm are shown in Figure 4C. Initially, no gain can be achieved with low fluence. With increasing fluence, the value of A turns negative after the initial short-lived positive feature caused by hot carriers[41] and an excitation threshold of ~20 μJ/cm^2 is extracted. Significant amplification is observed at a pump fluence of 40 μJ/cm^2 with a minimum absorbance value of −2.8 mOD and the optical gain relaxation can be fitted to a biexponential decay. Please note that, besides the fast component with a lifetime of 8.67 ± 0.2 ps, which is possibly due to the nonradiative Auger effect,[21] the slow decay component with a

lifetime of ~187 ± 5 ps matches well with the emission decay probed at 528 nm (~128 ± 17 ps in Figure 3C), confirming again the existence of emissive high-order excitonic states in Cu-doped CdSe CQWs.[5,44] Furthermore, it is worth mentioning that, with Cu-doped CQWs embedded in the Fabry-Pérot cavity, we have also successfully demonstrated lasing from the observed many-body correlations.[48]

In summary, we have demonstrated spectrally resolved, CW-pumped high-order excitonic emission in Cu-doped CdSe CQWs at room temperature, which is verified by the quadratic scaling with excitation of static emission intensity and the transient photophysical properties of many-body correlations. The presence of dopant excitons with ultralong lifetime and highly localized wavefunctions enables the efficient formation of many-body correlations with enhanced binding energy. We emphasize that the observed binding energy is up to 2-fold of those reported in other colloidal nanocrystals, and the demonstration of CW-pumped high-order excitonic emission stands out. The pumping level at ~10 W/cm^2 matches the power density of concentrated sunlight and correspond to an electrical density of ~5 A/cm^2, a level that could be attained in state-of-the-art DC-driven, light-emitting diodes with the colloidal nanomaterials. Thus, this work suggests that Cu-doped CQWs offer unique prospects for the design of novel solution-processable solid-state devices.

EXPERIMENTAL PROCEDURES

Resource availability

Lead contact

Further information and requests for resources should be directed to and will be fulfilled by the lead contact, Cuong Dang (hcdang@ntu.edu.sg).

Materials availability

The materials in this study will be made available upon reasonable request.

Data and code availability

The published article and its supplemental information include all data generated or analyzed during this study.

Estimation of the Cu atomic level

With ICP-MS we estimated Cu atomic levels with respect to cadmium and selenium. The average dimensions of our 4 ML cCu-doped CdSe CQWs measured by TEM microscopy are (40.3 ± 1.6) × (17.3 ± 2.9) × 1.2 nm, which suggests ~17,430 cadmium and ~13,695 selenium atoms in one CQW. Therefore, using ICP-MS measurements, we can estimate Cu atoms per CQW.

CW pumping PL spectroscopy

The CW excitation PL study was performed with a diode laser (Cobolt 06-MLD; excitation wavelength: 405 nm) and a fiber-coupled ANDOR spectrometer (monochromator: Andor Shamrock 303i, CCD: Andor iDus 401). Samples were drop-cast on a glass substrate for both room- and low-temperature measurements. The measurements were conducted in a surface emission geometry to avoid the spectra shift caused by reabsorption. The excitation spot radius is 50 μm, produced by a plano-concave lens with a focal length of 75 mm. For the low-temperature CW PL measurements, samples were cooled with a closed-cycle helium cryostat.

Calculation of the biexciton binding energy based on emission spectra

The biexciton binding energy is defined as the energy difference between biexciton states and two free excitons: $\Delta_{biex} = 2E_{ex} - E_{biex}$, where Δ_{biex} is the biexciton binding

energy, and E_{ex} and E_{biex} are the energies of the excitons and biexcitons, respectively. Considering that the radiative recombination of one biexciton will generate one exciton and emit one photon: $E_{biex} = E_{ex} + h\nu_{xx} = h\nu_x + h\nu_{xx}$ ($h\nu_x$ and $h\nu_{xx}$ are the photon energies of exciton and biexciton emission, respectively). Thus, one can calculate the biexciton binding energy (Δ_{biex}) based on the spectra shift: $\Delta_{biex} = h\nu_x - h\nu_{xx}$.

Time-resolved PL measurement

Time-resolved PL (trPL) measurements were performed using a streak camera from Optronics. The 400-nm pump laser pulses for trPL were generated by a 1,000 Hz regenerative amplifier (Coherent Libra). The beam from the regenerative amplifier has a center wavelength at 800 nm, a pulse width of around 150 fs, and was seeded by a mode-locked Ti-sapphire oscillator (Coherent Vitesse, 80 MHz). A 400-nm pump laser was obtained by frequency doubling the 800-nm fundamental regenerative amplifier output using a BBO crystal. All measurements were performed in the solid film at room temperature under ambient air (53% $\pm$ 2% humidity) conditions.

Transient absorption spectroscopy

Transient absorption (TA) spectroscopy was performed using a Helios setup (Ultrafast Systems) and in transmission mode with chirp correction. The white light continuum probe beam (in the range of 400–800 nm) was generated from a 3-mm sapphire crystal using 800-nm pulses from the regenerative amplifier, as described in the trPL measurement. The pump beam spot size is ~0.5 mm. The probe beam passing through the sample was collected using a detector for UV-vis (CMOS sensor). All measurements were performed at room temperature in solution (hexane).

SUPPLEMENTAL INFORMATION

Supplemental information can be found online at https://doi.org/10.1016/j.xcrp.2022.101049.

ACKNOWLEDGMENTS

C.D. is grateful for the financial support from the Ministry of Education, Singapore, under its AcRF Tier 2 grant (MOE-T2EP50121-0012). H.V.D. acknowledges the financial support in part from the Singapore Agency for Science, Technology and Research (A*STAR) MTC program under grant no. M21J9b0085, the Ministry of Education, Singapore, under its Academic Research Fund Tier 1 (MOE-RG62/20), and in part from TUBITAK 119N343, 20AG001, 121N395, and 121C266. H.V.D. also acknowledges support from TUBA and TUBITAK 2247-A National Leader Researchers Program (121C266). M.S. also acknowledges the funding through the Australian Research Council Center of Excellence in Exciton Science (grant no. CE170100026). We would like to thank Muhammad Taimoor and Thomas Kusserow at the University of Kassel (Kassel, Germany) for carefully reading our manuscript.

AUTHOR CONTRIBUTIONS

C.D. and H.V.D. supervised and contributed to all aspects of the research. J.Y., M.S., H.V.D., and C.D. wrote the manuscript. J.Y. conducted the spectroscopy measurements and initiated the study. M.S. performed the material syntheses and designed them to achieve the best performance. S.D. and A.S. helped in material synthesis and characterizations. M.L. performed trPL and transient absorption measurements. M.L. and T.C.S. supervised the ultrafast dynamic analysis. P.L.H.-M. helped to explain the experimental observations. Y.A. conducted the ICP-MS and XPS measurements. B.L. provided fruitful discussions about many-body physics. All authors

analyzed the data, discussed the results, commented on the manuscript, and participated in manuscript revision.

DECLARATION OF INTERESTS

The authors declare no competing interests.

Received: June 8, 2022
Revised: July 21, 2022
Accepted: August 22, 2022
Published: September 21, 2022

REFERENCES

1. Chen, S.-Y., Goldstein, T., Taniguchi, T., Watanabe, K., and Yan, J. (2018). Coulomb-bound four- and five-particle intervalley states in an atomically-thin semiconductor. Nat. Commun. *9*, 3717. https://doi.org/10.1038/s41467-018-05558-x.

2. Kira, M., and Koch, S.W. (2006). Many-body correlations and excitonic effects in semiconductor spectroscopy. Prog. Quant. Electron. *30*, 155–296. https://doi.org/10.1016/j.pquantelec.2006.12.002.

3. Grim, J.Q., Christodoulou, S., Di Stasio, F., Krahne, R., Cingolani, R., Manna, L., and Moreels, I. (2014). Continuous-wave biexciton lasing at room temperature using solution-processed quantum wells. Nat. Nanotechnol. *9*, 891–895. https://doi.org/10.1038/nnano.2014.213.

4. Chen, J., Zhang, Q., Shi, J., Zhang, S., Du, W., Mi, Y., Shang, Q., Liu, P., Sui, X., Wu, X., et al. (2019). Room temperature continuous-wave excited biexciton emission in perovskite nanoplatelets via plasmonic nonlinear fano resonance. Commun. Phys. *2*, 80. https://doi.org/10.1038/s42005-019-0178-9.

5. You, Y., Zhang, X.-X., Berkelbach, T.C., Hybertsen, M.S., Reichman, D.R., and Heinz, T.F. (2015). Observation of biexcitons in monolayer WSe2. Nat. Phys. *11*, 477–481. https://doi.org/10.1038/nphys3324.

6. Peng, L., Otten, M., Hazarika, A., Coropceanu, I., Cygorek, M., Wiederrecht, G.P., Hawrylak, P., Talapin, D.V., and Ma, X. (2020). Bright trion emission from semiconductor nanoplatelets. Phys. Rev. Mater. *4*, 056006. https://doi.org/10.1103/PhysRevMaterials.4.056006.

7. Delteil, A., Sun, Z., Gao, W.-b., Togan, E., Faelt, S., and Imamoğlu, A. (2016). Generation of heralded entanglement between distant hole spins. Nat. Phys. *12*, 218–223. https://doi.org/10.1038/nphys3605.

8. Soumyanarayanan, A., Reyren, N., Fert, A., and Panagopoulos, C. (2016). Emergent phenomena induced by spin–orbit coupling at surfaces and interfaces. Nature *539*, 509–517. https://doi.org/10.1038/nature19820.

9. Yu, J., Sharma, M., Sharma, A., Delikanli, S., Volkan Demir, H., and Dang, C. (2020). All-optical control of exciton flow in a colloidal quantum well complex. Light Sci. Appl. *9*, 27. https://doi.org/10.1038/s41377-020-0262-7.

10. Geiregat, P., Rodá, C., Tanghe, I., Singh, S., Di Giacomo, A., Lebrun, D., Grimaldi, G., Maes, J., Van Thourhout, D., Moreels, I., et al. (2021). Localization-limited exciton oscillator strength in colloidal CdSe nanoplatelets revealed by the optically induced Stark effect. Light Sci. Appl. *10*, 112. https://doi.org/10.1038/s41377-021-00548-z.

11. Yu, J., Hou, S., Sharma, M., Tobing, L.Y., Song, Z., Delikanli, S., Hettiarachchi, C., Zhang, D., Fan, W., Birowosuto, M.D., et al. (2020). Strong plasmon-wannier mott exciton interaction with high aspect ratio colloidal quantum wells. Matter *2*, 1550–1563. https://doi.org/10.1016/j.matt.2020.03.013.

12. Winkler, J.M., Rabouw, F.T., Rossinelli, A.A., Jayanti, S.V., McPeak, K.M., Kim, D.K., le Feber, B., Prins, F., and Norris, D.J. (2019). Room-temperature strong coupling of CdSe nanoplatelets and plasmonic hole arrays. Nano Lett. *19*, 108–115. https://doi.org/10.1021/acs.nanolett.8b03422.

13. Flatten, L.C., Christodoulou, S., Patel, R.K., Buccheri, A., Coles, D.M., Reid, B.P.L., Taylor, R.A., Moreels, I., and Smith, J.M. (2016). Strong exciton–photon coupling with colloidal nanoplatelets in an open microcavity. Nano Lett. *16*, 7137–7141. https://doi.org/10.1021/acs.nanolett.6b03433.

14. Ithurria, S., Tessier, M.D., Mahler, B., Lobo, R.P.S.M., Dubertret, B., and Efros, A.L. (2011). Colloidal nanoplatelets with two-dimensional electronic structure. Nat. Mater. *10*, 936–941. https://doi.org/10.1038/nmat3145.

15. Ithurria, S., Bousquet, G., and Dubertret, B. (2011). Continuous transition from 3D to 1D confinement observed during the formation of CdSe nanoplatelets. J. Am. Chem. Soc. *133*, 3070–3077. https://doi.org/10.1021/ja110046d.

16. Yu, J., and Dang, C. (2021). Colloidal metal chalcogenide quantum wells for laser applications. Cell Rep. Phys. Sci. *2*, 100308. https://doi.org/10.1016/j.xcrp.2020.100308.

17. Li, Q., Xu, Z., McBride, J.R., and Lian, T. (2017). Low threshold multiexciton optical gain in colloidal CdSe/CdTe core/crown type-II nanoplatelet heterostructures. ACS Nano *11*, 2545–2553. https://doi.org/10.1021/acsnano.6b08674.

18. Rowland, C.E., Fedin, I., Zhang, H., Gray, S.K., Govorov, A.O., Talapin, D.V., and Schaller, R.D. (2015). Picosecond energy transfer and multiexciton transfer outpace Auger recombination in binary CdSe nanoplatelet solids. Nat. Mater. *14*, 484–489. https://doi.org/10.1038/nmat4231.

19. Shornikova, E.V., Yakovlev, D.R., Biadala, L., Crooker, S.A., Belykh, V.V., Kochiev, M.V., Kuntzmann, A., Nasilowski, M., Dubertret, B., and Bayer, M. (2020). Negatively charged excitons in CdSe nanoplatelets. Nano Lett. *20*, 1370–1377. https://doi.org/10.1021/acs.nanolett.9b04907.

20. Antolinez, F.V., Rabouw, F.T., Rossinelli, A.A., Keitel, R.C., Cocina, A., Becker, M.A., and Norris, D.J. (2020). Trion emission dominates the low-temperature photoluminescence of CdSe nanoplatelets. Nano Lett. *20*, 5814–5820. https://doi.org/10.1021/acs.nanolett.0c01707.

21. Li, Q., and Lian, T. (2017). Area- and thickness-dependent biexciton auger recombination in colloidal CdSe nanoplatelets: breaking the "universal volume scaling law". Nano Lett. *17*, 3152–3158. https://doi.org/10.1021/acs.nanolett.7b00587.

22. Ye, Z., Waldecker, L., Ma, E.Y., Rhodes, D., Antony, A., Kim, B., Zhang, X.-X., Deng, M., Jiang, Y., Lu, Z., et al. (2018). Efficient generation of neutral and charged biexcitons in encapsulated WSe2 monolayers. Nat. Commun. *9*, 3718. https://doi.org/10.1038/s41467-018-05917-8.

23. Robert, C. (2018). When bright and dark bind together. Nat. Nanotechnol. *13*, 982–983. https://doi.org/10.1038/s41565-018-0281-1.

24. Han, Y., He, S., Luo, X., Li, Y., Chen, Z., Kang, W., Wang, X., and Wu, K. (2019). Triplet sensitization by "self-trapped" excitons of nontoxic CuInS2 nanocrystals for efficient photon upconversion. J. Am. Chem. Soc. *141*, 13033–13037. https://doi.org/10.1021/jacs.9b07033.

25. Stébé, B., Assaid, E., Dujardin, F., and Goff, S.L. (1996). Exciton bound to an ionized donor impurity in semiconductor spherical quantum dots. Phys. Rev. B Condens. Matter *54*, 17785–17793. https://doi.org/10.1103/PhysRevB.54.17785.

26. Yu, J., Sharma, M., Wang, Y., Delikanli, S., Baruj, H.D., Sharma, A., Demir, H.V., and Dang, C. (2022). Modulating emission properties in a host–guest colloidal quantum well superlattice. Adv. Opt. Mater. *10*, 2101756. https://doi.org/10.1002/adom.202101756.

27. Sharma, M., Gungor, K., Yeltik, A., Olutas, M., Guzelturk, B., Kelestemur, Y., Erdem, T., Delikanli, S., McBride, J.R., and Demir, H.V.

(2017). Near-unity emitting copper-doped colloidal semiconductor quantum wells for luminescent solar concentrators. Adv. Mater. *29*, 1700821. https://doi.org/10.1002/adma.201700821.

28. Yu, J., Sharma, M., Delikanli, S., Birowosuto, M.D., Demir, H.V., and Dang, C. (2019). Mutual energy transfer in a binary colloidal quantum well complex. J. Phys. Chem. Lett. *10*, 5193–5199. https://doi.org/10.1021/acs.jpclett.9b01939.

29. Sharma, M., Olutas, M., Yeltik, A., Kelestemur, Y., Sharma, A., Delikanli, S., Guzelturk, B., Gungor, K., McBride, J.R., and Demir, H.V. (2018). Understanding the journey of dopant copper ions in atomically flat colloidal nanocrystals of CdSe nanoplatelets using partial cation exchange reactions. Chem. Mater. *30*, 3265–3275. https://doi.org/10.1021/acs.chemmater.8b00196.

30. Hughes, K.E., Hartstein, K.H., and Gamelin, D.R. (2018). Photodoping and transient spectroscopies of copper-doped CdSe/CdS nanocrystals. ACS Nano *12*, 718–728. https://doi.org/10.1021/acsnano.7b07879.

31. Galle, T., Kazes, M., Hübner, R., Lox, J., Samadi Khoshkhoo, M., Sonntag, L., Tietze, R., Sayevich, V., Oron, D., Koitzsch, A., et al. (2019). Colloidal mercury-doped CdSe nanoplatelets with dual fluorescence. Chem. Mater. *31*, 5065–5074. https://doi.org/10.1021/acs.chemmater.9b00812.

32. Khan, A.H., Pinchetti, V., Tanghe, I., Dang, Z., Martín-García, B., Hens, Z., Van Thourhout, D., Geiregat, P., Brovelli, S., and Moreels, I. (2019). Tunable and efficient red to near-infrared photoluminescence by synergistic exploitation of core and surface silver doping of CdSe nanoplatelets. Chem. Mater. *31*, 1450–1459. https://doi.org/10.1021/acs.chemmater.8b05334.

33. Tenne, R., Pedetti, S., Kazes, M., Ithurria, S., Houben, L., Nadal, B., Oron, D., and Dubertret, B. (2016). From dilute isovalent substitution to alloying in CdSeTe nanoplatelets. Phys. Chem. Chem. Phys. *18*, 15295–15303. https://doi.org/10.1039/C6CP01177B.

34. Saidzhonov, B.M., Zaytsev, V.B., Berekchiian, M.V., and Vasiliev, R.B. (2020). Highly luminescent copper-doped ultrathin CdSe nanoplatelets for white-light generation. J. Lumin. *222*, 117134. https://doi.org/10.1016/j.jlumin.2020.117134.

35. Nelson, H.D., Hinterding, S.O.M., Fainblat, R., Creutz, S.E., Li, X., and Gamelin, D.R. (2017). Mid-gap states and normal vs inverted bonding in luminescent Cu+- and Ag+-Doped CdSe nanocrystals. J. Am. Chem. Soc. *139*, 6411–6421. https://doi.org/10.1021/jacs.7b01924.

36. Diroll, B.T., Cho, W., Coropceanu, I., Harvey, S.M., Brumberg, A., Holtgrewe, N., Crooker, S.A., Wasielewski, M.R., Prakapenka, V.B., Talapin, D.V., and Schaller, R.D. (2018). Semiconductor nanoplatelet excimers. Nano Lett. *18*, 6948–6953. https://doi.org/10.1021/acs.nanolett.8b02865.

37. Yu, J., Han, Y., Zhang, H., Ding, X., Qiao, L., and Hu, J. (2022). Excimer formation in the non-van-der-waals 2D semiconductor Bi2O2Se. Adv. Mater. 2204227. https://doi.org/10.1002/adma.202204227.

38. Wang, Y., Li, X., Song, J., Xiao, L., Zeng, H., and Sun, H. (2015). All-inorganic colloidal perovskite quantum dots: a new class of lasing materials with favorable characteristics. Adv. Mater. *27*, 7101–7108. https://doi.org/10.1002/adma.201503573.

39. Utzat, H., Sun, W., Kaplan, A.E.K., Krieg, F., Ginterseder, M., Spokoyny, B., Klein, N.D., Shulenberger, K.E., Perkinson, C.F., Kovalenko, M.V., and Bawendi, M.G. (2019). Coherent single-photon emission from colloidal lead halide perovskite quantum dots. Science *363*, 1068–1072. https://doi.org/10.1126/science.aau7392.

40. Lim, J., Park, Y.-S., and Klimov, V.I. (2018). Optical gain in colloidal quantum dots achieved with direct-current electrical pumping. Nat. Mater. *17*, 42–49. https://doi.org/10.1038/nmat5011.

41. Geiregat, P., Houtepen, A.J., Sagar, L.K., Infante, I., Zapata, F., Grigel, V., Allan, G., Delerue, C., Van Thourhout, D., and Hens, Z. (2018). Continuous-wave infrared optical gain and amplified spontaneous emission at the ultralow threshold by colloidal HgTe quantum dots. Nat. Mater. *17*, 35–42. https://doi.org/10.1038/nmat5000.

42. Hao, K., Specht, J.F., Nagler, P., Xu, L., Tran, K., Singh, A., Dass, C.K., Schüller, C., Korn, T., Richter, M., et al. (2017). Neutral and charged inter-valley biexcitons in monolayer MoSe2. Nat. Commun. *8*, 15552. https://doi.org/10.1038/ncomms15552.

43. Bacher, G., Weigand, R., Seufert, J., Kulakovskii, V.D., Gippius, N.A., Forchel, A., Leonardi, K., and Hommel, D. (1999). Biexciton versus exciton lifetime in a single semiconductor quantum dot. Phys. Rev. Lett. *83*, 4417–4420. https://doi.org/10.1103/PhysRevLett.83.4417.

44. Spiegel, R., Bacher, G., Forchel, A., Jobst, B., Hommel, D., and Landwehr, G. (1997). Polarization-dependent formation of biexcitons in (Zn, Cd)Se/ZnSe quantum wells. Phys. Rev. B *55*, 9866–9871. https://doi.org/10.1103/PhysRevB.55.9866.

45. Soavi, G., Dal Conte, S., Manzoni, C., Viola, D., Narita, A., Hu, Y., Feng, X., Hohenester, U., Molinari, E., Prezzi, D., et al. (2016). Exciton–exciton annihilation and biexciton stimulated emission in graphene nanoribbons. Nat. Commun. *7*, 11010. https://doi.org/10.1038/ncomms11010.

46. Sutherland, B.R., Hoogland, S., Adachi, M.M., Kanjanaboos, P., Wong, C.T.O., McDowell, J.J., Xu, J., Voznyy, O., Ning, Z., Houtepen, A.J., and Sargent, E.H. (2015). Perovskite thin films via atomic layer deposition. Adv. Mater. *27*, 53–58. https://doi.org/10.1002/adma.201403965.

47. Yu, J., Shendre, S., Koh, W.-k., Liu, B., Li, M., Hou, S., Hettiarachchi, C., Delikanli, S., Hernández-Martínez, P., Birowosuto, M.D., et al. (2019). Electrically control amplified spontaneous emission in colloidal quantum dots. Sci. Adv. *5*, 3140. https://doi.org/10.1126/sciadv.aav3140.

48. Yu, J., Sharma, M., Li, M., Delikanli, S., Sharma, A., Taimoor, M., Altintas, Y., McBride, J.R., Kusserow, T., Sum, T., et al. (2021). Low-threshold lasing from copper-doped CdSe colloidal quantum wells. Laser Photon. Rev. *15*, 2100034. https://doi.org/10.1002/lpor.202100034.